NASA TECHNICAL NOTE

NASA TN D-3160

NASA TN D-3160

ATOMIC BEAM DETERMINATION OF THE CESIUM-CESIUM TOTAL SCATTERING CROSS SECTION

by John W. Sheldon and Eugene J. Manista

Lewis Research Center
Cleveland, Ohio

NATIONAL AERONAUTICS AND SPACE ADMINISTRATION • WASHINGTON, D. C. • DECEMBER 1965

NASA TN D-3160

ATOMIC BEAM DETERMINATION OF THE CESIUM-CESIUM TOTAL SCATTERING CROSS SECTION

By John W. Sheldon and Eugene J. Manista

Lewis Research Center
Cleveland, Ohio

NATIONAL AERONAUTICS AND SPACE ADMINISTRATION

For sale by the Clearinghouse for Federal Scientific and Technical Information
Springfield, Virginia 22151 – Price $2.00

ATOMIC BEAM DETERMINATION OF THE CESIUM-CESIUM TOTAL SCATTERING CROSS SECTION

by John W. Sheldon and Eugene J. Manista

Lewis Research Center

SUMMARY

The cesium-cesium cross section is measured at three angular resolutions in the laboratory by total beam transmission through a scattering chamber containing cesium scattering atoms. The results show a marked dependence on laboratory angular resolution indicative of strong forward scattering. The forward scattering peak in the differential cross section is further evidenced by observations of broadening in the attenuated beam. The effective cross sections determined in the attenuations are correlated with an inverse r-sixth interaction and reduced to partial cross sections using the Berkling et al. tables. The partial cross sections are further analyzed within the framework of the semiclassical theory of Mason, Vanderslice, and Raw to obtain a method of extrapolation to zero angle in order to yield the total cross section corresponding to the assumed interaction $V(r) = -C/r^6$, where $V(r)$ is the interaction potential, C is the dispersion energy constant, and r is the interatomic distance. The total cross section determined by this method for cesium-cesium is 2500 Å^2 at a relative velocity of 2.3×10^4 centimeters per second. From the value of the cross section an interaction strength of $C = 4080\times10^{-60}$ erg-cm^6 is calculated from the Schiff, Landau-Lifschitz relation. The ratio of experimental to theoretical value of C is within the usual factor of 2 range found for other beam-gas interaction pairs.

INTRODUCTION

The scattering of a collimated beam of particles by target particles has long been recognized as an effective method of obtaining information about the strength and range of interactions between particles. At thermal energies, a variety of atomic beam techniques are available to study the intermolecular interactions (for recent review articles see Bernstein, ref. 1, and Pauly, ref. 2). The quantity often measured in these experi-

ments is the absolute magnitude of the collision cross section. A large number of beam and target particle combinations have recently been investigated by using these methods, and the magnitudes of the cross sections have been found to be consistently larger than those predicted by theoretical cross-section calculations (Rothe and Bernstein (ref. 3), Rothe et al. (ref. 4), and Pauly (ref. 5)).

A possible source of experimental error that may reduce these discrepancies involves the use of liquid nitrogen trapped McLeod gages to determine the absolute pressure and hence the density of scattering particles participating in the collisions. The error in using the McLeod gage in this manner arises, as pointed out by Ishii and Nakayama (ref. 6) and Meinke and Reich (ref. 7), because the steady stream of mercury vapor between the McLeod gage and the cold trap acts as a small diffusion pump that tends to reduce the pressure in the body of the McLeod gage; therefore, the indicated pressure underestimates the actual pressure in the system. This problem was not encountered in the investigation reported herein, since a McLeod gage was not used for pressure measurement.

Another source of experimental error is that associated with the laboratory angular resolving power, that is, the ability of the experimental arrangement to detect the small angle collisions that deflect an incident beam particle out of the transmitted beam. Pauly (ref. 8) has studied the effect of differential scattering at small angles by using mercury as the scattering gas and sodium and potassium as the beam particles. The results show the strong forward scattering characteristic of van der Waals (inverse sixth power) long range attraction and furthermore illustrate the laboratory angular resolution necessary in order to be reasonably certain that the cross section measured is indeed the total cross section.

The cesium-cesium total cross section was first measured by Estermann, Foner, and, Stern (ref. 9). They obtained a value of 2350 $Å^2$ for the hard-sphere cross section*. A reevaluation of their data using the Berkling et al. (ref. 10) tables for velocity-dependent cross sections** increases their original value by 6 percent or to 2500 $Å^2$ at a relative velocity of 3.9×10^4 centimeters per second.

A more meaningful quantity to compare with theoretical calculations is the value of the constant C in the dispersion energy ($V(r) = -C/r^6$ for van der Waals forces) rather than the cross section. The constant C in erg-cm^6 can be calculated from the Schiff, Landau-Lifschitz approximation $C = 5.676\times10^{-30}\, vQ^{5/2}$, where v, the relative collision velocity, is in centimeters per second and Q, the experimental cross section, is in

---

*Actually this cross section is for a monoenergetic cesium atom of velocity 3.9×10^4 cm/sec incident into a cesium vapor at a temperature of about 350° K.

**Estermann et al. at the time had tables available only for the velocity-independent hard-sphere cross section.

square centimeters. When the corrected velocity-dependent cross section of Estermann et al. is used, a value of 6900×10^{-60} erg-cm^6 is obtained for C. This may be compared to the recent theoretical calculations of Fontana (ref. 11); he computed C to be about 2200×10^{-60} erg-cm^6 for the long-ranged cesium-cesium interaction at thermal energies. Since the experimental C values determined for other beam-scattering gas combinations are usually about a factor of two larger than the theoretical values (Bernstein, ref. 12), the large cross section for cesium-cesium appears to be an anomaly.

The above discrepancy as well as the current interest in cesium for gaseous electronic devices has prompted the remeasurement of this cross section. The measurement is based on standard molecular beam transmission techniques wherein the incident beam becomes increasingly attenuated as the density of scattering particles in the scattering region is increased. The scattering atom density is measured directly by observing the particle flux effusing from the scattering chamber. The assumption that the angular resolution is sufficient to measure the total cross section is not made, rather the apparent "total" cross section (hereafter referred to as the partial cross section) is measured as a function of the angular resolution of the apparatus. The results are analyzed within the framework of the semiclassical theory of Mason, Vanderslice, and Raw (ref. 13) in order to extrapolate the measured partial cross sections to zero scattering angle and hence obtain a value of the true total cross section.

The conversion of the scattering angle in the center of mass system to the appropriate angle in the laboratory system is required in the extrapolation. This transformation as well as the velocity-averaging procedure employed is described in appendix C for small scattering angles.

COMPARISON OF CLASSICAL AND SEMICLASSICAL CROSS-SECTION CALCULATIONS

In this section, a summary of the results of applying various methods of calculation of the cross section from an assumed interaction energy is given. The ranges of validity of the various approaches are discussed, and the method of performing the extrapolation of the partial cross section to zero scattering angle is developed.

The interaction between two ground-state cesium atoms, the case treated herein, can actually proceed along two different interaction curves depending on the spin orientations of the colliding atoms. Sketch (a) (p. 4) shows the qualitative features of the singlet and triplet interactions (ref. 14). However, since small angle scattering events are of primary interest, that is, long range forces are dominant, the singlet-triplet splitting is negligible and the interaction is well approximated at large values of r by an inverse r-sixth potential.

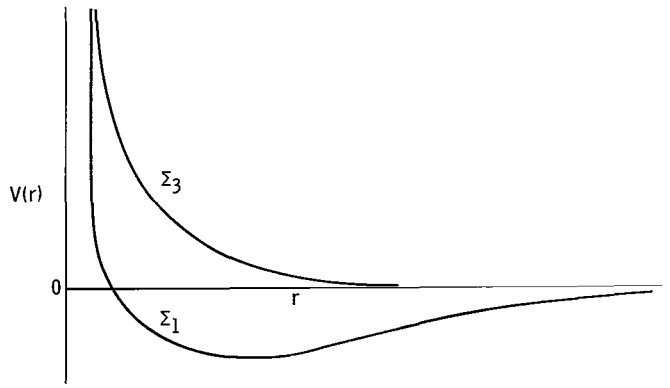

(a)

The differential scattering cross section $\sigma(\theta)$ computed by the methods of classical mechanics for an interaction potential $V(r)$ of the form

$$V(r) = \pm \frac{K}{r^s} \tag{1}$$

is given by Mason, Vanderslice, and Raw (ref. 13) as

$$\sigma(\theta) = \frac{1}{s}\left(\frac{KC_s}{\epsilon}\right)^{2/s}\left(\frac{1}{\theta}\right)^{\frac{2s+2}{s}} \tag{2}$$

where $\epsilon = 1/2\ \mu\langle v_r\rangle^2$, μ is the reduced mass, $\langle v_r\rangle$ is the average relative velocity of the colliding particles, θ is the angle through which the particles are scattered in the center of mass system, and

$$C_s = \frac{\pi^{1/2}\Gamma\left(\frac{s+1}{2}\right)}{\Gamma\left(\frac{s}{2}\right)}$$

(All symbols are defined in appendix A.)

The total cross section $S(0)$ is defined in terms of the differential scattering cross section by

$$S(0) = 2\pi \int_0^{\pi} \sigma(\theta)\sin\theta\, d\theta \tag{3}$$

The use of the classical expression (eq. (2)) for the differential cross section $\sigma(\theta)$ in equation (3) gives an infinite result for $S(0)$. The result is not surprising as it has long been recognized that classical mechanics fails to provide the proper description of small angle scattering. Massey and Mohr (ref. 15) have pointed out that $S(0)$ is finite because of quantum effects. If $\theta < \theta_c$ where

$$\theta_c \cong \pi\left[\frac{2\pi}{S(0)}\right]^{1/2} \frac{\hbar}{\mu\langle v_r\rangle} \tag{4}$$

($\hbar$ is Planck's constant divided by 2π), then according to Massey and Mohr classical mechanics can no longer be used to describe the scattering. Even for $\theta > \theta_c$, classical results only give a mean value for the angular dependence of the differential scattering cross section (Ford and Wheeler, ref. 16).

Recently, Mason et al. (ref. 13) have derived a semiclassical expression for $\sigma(\theta)$ that is valid for angles $\theta < \theta_c$ and which approaches the classical value as θ approaches θ_c. Their semiclassical expression approaches a constant as θ goes to zero and hence can be used to obtain a finite estimate of $S(0)$. The result of reference 13 applied to an inverse r-sixth potential is given in the following:

$$\sigma(\theta) = |f(\theta)|^2 \tag{5a}$$

$$|f(\theta)| \simeq \left[\frac{kS(0)}{4\pi}\right]\left[\sec\left(\frac{\pi}{5}\right)\right]\exp\left[-\frac{f(6)k^2S(0)\theta^2}{16\pi}\right] \tag{5b}$$

where $|f(\theta)|$ is the magnitude of the small angle semiclassical scattering amplitude, k is the wave number given by

$$k = \frac{\mu\langle v_r\rangle}{\hbar}$$

and

$$f(6) = \frac{\left[\Gamma\left(\frac{2}{5}\right)\right]^2}{2\pi\Gamma\left(\frac{4}{5}\right)} \tan\left(\frac{2\pi}{5}\right)$$

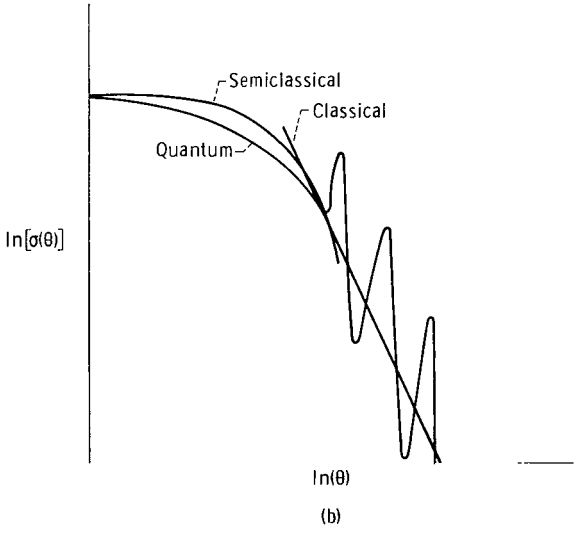

(b)

The behavior of the differential cross section as described by classical, semiclassical, and quantum mechanics is shown in sketch (b). Mason et al. also point out that classical mechanics is valid down to smaller angles than was indicated by Massey

and Mohr. The criterion of Mason et al. for the validity of classical mechanics is that the classical expression (eq. (2)) can be used for angles $\theta > \theta'_c$ where

$$\theta'_c \cong \frac{\theta_c}{\pi} \tag{6}$$

The atomic beam transmission technique measures the amount of scattering of incident beam atoms through angles greater than some small angle θ_L in the laboratory system (the angular resolution of the apparatus). Since the theoretical cross sections are given in terms of quantities in the center of mass system, it is necessary to transform the angle θ_L in the laboratory to the corresponding angle in the center of mass system before comparing the results of the measurement with theory. The transformation depends on the kinematics of the collision and also on the velocities of the colliding particles. Moreover, the transformation must be averaged over the velocity distribution present in the beam and also over the velocity distribution present in the scattering gas. This average over velocities introduces uncertainty into the method due to the lack, in some collisions, of a one-to-one correspondence between the scattered angle in the laboratory system and the corresponding angle in the center of mass system. The transformation and velocity averaging are indicated in appendix C. The result obtained for small angles is

$$\theta^2_{cm} \cong \frac{4\left\langle \theta^2_L \right\rangle}{1 + \frac{1}{2}\frac{T_g}{T_b}} \tag{7}$$

where θ^2_{cm} is the square of the scattering angle in the center of mass system associated with the average square of the laboratory angle $\left\langle \theta^2_L \right\rangle$. The above result is only valid for equal mass collision partners and for Maxwellian-type beam and scattering gas particles where T_g is the kinetic temperature of the scattering gas particles and T_b is the kinetic temperature of the beam particles.

If $\theta'_c < \theta_{cm} < \theta_c$, as is the case for the experiments reported herein, then both the classical (eq. (2)) and semiclassical (eq. (5a)) expressions should give fair approximations to the differential cross section.

The cross section for deflections through angles greater than θ_{cm} is referred to herein as the partial cross section $S(\theta_{cm})$ and is given by (see appendix B)

$$S(\theta_{cm}) = S(0) - 2\pi \int_0^{\theta_{cm}} \sigma(\theta) \sin\theta \, d\theta \tag{8}$$

When the classical differential cross section given by equation (2) is used in equation (8), one obtains (ref. 13)

$$S(\theta_{cm}) = \pi\left(\frac{KC_s}{\epsilon\theta_{cm}}\right)^{2/s} \tag{9}$$

Equation (9) is not valid for $\theta_{cm} < \theta'_c$ and therefore cannot be used in extrapolating to zero angle to obtain $S(0)$ from $S(\theta_{cm})$. An expression for $S(\theta_{cm})$ obtained from the semiclassical calculations can, however, be used for such an extrapolation. If the semiclassical expression for $\sigma(\theta)$, as given by equations (5a) and (5b), and the transformation equation (7) is used in equation (8), it can be placed in the following approximate form after integration:

$$\ln\left\{1 - \frac{2f(6)}{\left[1 + \tan^2\left(\frac{\pi}{5}\right)\right]}\left[1 - \frac{S(\theta_L)}{S(0)}\right]\right\} \simeq -\frac{f(6)k^2S(0)}{2\pi\left(1 + \frac{1}{2}\frac{T_g}{T_b}\right)}\theta_L^2 \tag{10}$$

Equation (5b) is only applicable for those center of mass angles $\theta < \theta_c$, or in the laboratory for those angles θ_L such that

$$\theta_L < \frac{\pi}{2k}\left[\frac{2\pi}{S(0)}\left(1 + \frac{1}{2}\frac{T_g}{T_b}\right)\right]^{1/2}$$

One might be concerned about the application of equation (5) to cesium-cesium collisions since reference 13 does not consider the special case of identical particles. In place of equation (5a), it would be more correct to write the differential cross section $\sigma(\theta)$ (ref. 15) as

$$\sigma(\theta) = \left|f(\theta)\right|^2 + \left|f(\pi - \theta)\right|^2 + \left\{A\ \mathrm{Re}\left[f(\theta)f(\pi - \theta)\right]\right\} \tag{5a'}$$

where A depends on the spin statistics of the colliding systems ($|A| \leq 2$). In order to estimate the relative values of the terms in equation (5a') for small values of θ, an expression for $f(\pi - \theta)$ when $(\pi - \theta)$ is near π is needed in addition to equation (5b). The classical approximation (eq. (2)) can be used here since $\pi - \theta > \theta_c$; that is,

$$|f(\pi - \theta)| \simeq \sqrt{\frac{1}{6}\left(\frac{KC_6}{\epsilon(\pi - \theta)^7}\right)^{1/3}} \qquad (11)$$

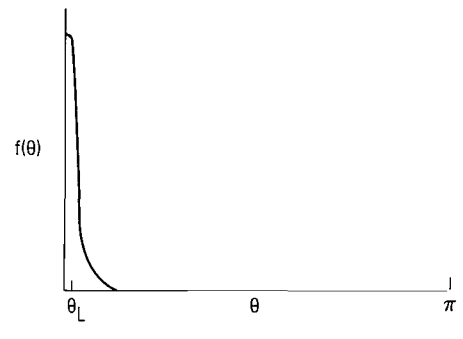

(c)

The scattering amplitude $f(\theta)$ as given by equation (5b) and equation (11) is shown in sketch (c). It can be seen from the above discussion that neglecting the last two terms of equation (5a') is justifiable, since for small values of θ

$$|f(\theta)| >> |f(\pi - \theta)|$$

EXPERIMENTAL METHOD

Apparatus and Procedure

The general features of the atomic beam facility have been described in an earlier report (Manista and Sheldon, ref. 17). Figure 1 shows the essential details and geometry of the experimental layout employed in the present investigation. The main oven O, the scattering chamber SC, and the scattering chamber reservoir SCR were made from solid blocks of high purity copper. In order to eliminate thermal conduction through base supports, these components were mounted on a Supramica base (thermal conductivity $\simeq 10^{-3}$ cal/(cm)(sec)(^{o}C)). The scattering chamber and the scattering chamber reservoir were connected by a thin-walled stainless-steel transfer tube. Each of the components was equipped with alternating-current heaters that were used to maintain the desired local temperatures. An extensive iron-constantan thermocouple system monitored and controlled the temperatures of each during the experimental runs.

The slits S_1, S_2, and S_3 were made from sheets of 0.051-millimeter-thick stainless-steel shim stock in which narrow slits of about 5 millimeters height were cut by an electron beam technique. Each slit plate was also provided with two slots cut at right angles to the 5-millimeter-high slit. These slots fitted onto dowel pins accurately located in the faces of the oven and the scattering chamber and facilitated the horizontal adjustment of the slits during alinement.

The detector D was a surface ionization type employing a 0.0554-millimeter-diameter tungsten filament positioned such that its length was along the vertical extent of the main beam. The detector could be moved at right angles across the horizontal extension of the main beam by means of a micrometer screw located outside the vacuum envelope. The relative reproducibility of the detector movement amounted to ±5 microns.

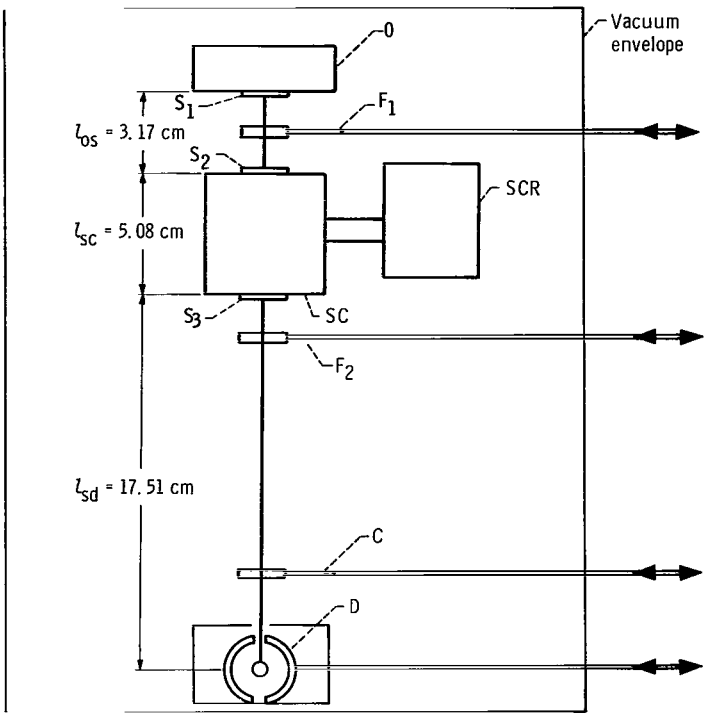

Run	S_1, cm	S_2, cm	S_3, cm	C, cm	D, cm
1	0.0045	0.0054	0.0041	0.10	0.0055
2a	.0041	.010	.020	.10	.0055
2b	.0041	.010	.020	.10	.0055
3	.011	.010	.011	.10	.0055

Height of S_1, S_2, and S_3 for all runs, 0.508 cm.
Height of C and D for all runs, 0.635 cm.

Figure 1. - Diagram (not to scale) of atomic beam apparatus showing geometric location of components. Main oven, O; scattering chamber, SC; scattering chamber reservoir, SCR; surface ionization detector, D; beam shutters, F_1 and F_2; collimator, C; oven slit, S_1; scattering chamber slits, S_2 and S_3.

The width of the detector filament and the widths of the slits were measured by comparison against a calibrated reticle under 300× magnification in a microscope. Use of the three sets of slits (fig. 1) gave a different experimental angular resolution for each of the three runs.

The slits S_1, S_2, and S_3 (fig. 1) were alined optically; an intense light source was placed in the main oven O, and the centerline of the beam was established by sighting into the oven with a cathotometer. The slits were then centered so as to fall on the cathotometer vertical hairline. Considerable care was taken to aline the slits horizontally and to insure that they were all vertically parallel with respect to each other. The cathotometer was also used to check the relative heights of S_1, S_2, S_3, C, and D. The

wide collimating slit C was positioned such that it did not influence the main beam profile (an exception is run 2b).

The apparatus was mounted in a 32-inch-diameter stainless-steel vacuum chamber that operated typically in the 1×10^{-7} torr range. Liquid nitrogen cold trapping and baffling were used to lower the concentration of cesium in the critical areas of the apparatus. A filament temperature of about 1800° K was used to surface ionize the incident cesium atoms, and 94 volts was used to collect the resulting ions. The ion current from the detector was measured by a Cary Model 31 electrometer whose output was recorded on a strip chart recorder.

High purity cesium (99.95 percent, material and analysis supplied by the Dow Chemical Co.), contained in vacuum-loaded pyrex ampoules, was used as the source material for both the main beam and the scattering vapor. The pyrex ampoules were placed in the well reservoirs of the oven and the scattering chamber reservoir prior to closing the chamber. Each reservoir was fitted with a plunger that ruptured the ampoules from the exterior of the chamber. After a thorough bakeout of the components (300° C for at least 24 hr), the temperature T_b of the beam oven O and the scattering chamber temperature T_{SC} were lowered and maintained at 155° and 110° C, respectively. The temperature of the cesium reservoir T_{SCR} was held at various values between 0° and 70° C during each run.

The procedure used and the data taken in a typical run were as follows. A constant main beam was first established through the scattering chamber while the scattering chamber reservoir was at a temperature of about 110° C (the cesium ampoule in the scattering chamber reservoir was not yet broken). The temperature of the scattering chamber reservoir was then reduced to 0° C while observing the intensity at the peak of the main beam. If the peak intensity did not increase appreciably during this cooling down period the outgassing of the scattering chamber reservoir was judged insignificant and the actual attenuation run was initiated. (Some actual spatial shifting of the entire beam occurred during the cool down period because of thermal effects; however, the intensity at the peak usually did not change by more than 2 percent). The unattenuated (100-percent transmission) profile of the main beam was measured by moving the detector stepwise across the beam and recording the corresponding detector current. The background level was observed by shuttering flag F_2 (fig. 1). The experimental half-width of the beam was needed to evaluate the angular resolution of the arrangement (to be discussed subsequently). The detector was then brought back to the position of the peak beam intensity and the temperature of the scattering chamber reservoir was increased to about 70° C. At this time, the cesium ampoule in the scattering chamber reservoir was broken. This high reservoir temperature enabled the cesium to coat the walls of the scattering chamber and the scattering chamber reservoir relatively quickly (about 15 min).

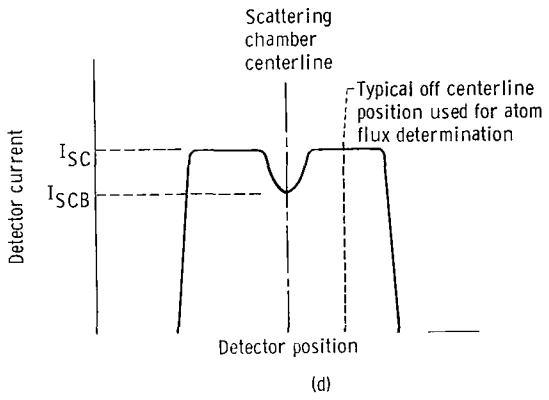

(d)

Since the scattering chamber containing the cesium scattering atoms also acted as an oven, a point on the attenuation line was determined in the following manner. The current measured at the peak of the main beam profile with both flags F_1 and F_2 open (fig. 1) was denoted by I_{BT}. This current I_{BT} was actually composed of the attenuated beam current I_B plus an additional current I_{SCB} due to the flux of cesium scattering atoms from the scattering chamber. The density of cesium scattering atoms was measured by observing the flux from the scattering chamber exit slit S_3 that was indicative of the flux from an ideal isothermal enclosure. This flux measurement was made by blocking the main beam with flag F_1 and moving the detector D off the scattering chamber centerline such that it could not "see" the scattering chamber entrance slit. The atom flux profile from the scattering chamber with F_1 blocking the main beam is shown in sketch (d). Moving D to the off-center position illustrated in sketch (d) gave a measurement of the atom flux from an ideal isothermal enclosure (Manista and Sheldon, ref. 18). The detected current at this off-center position was denoted by I_{SCT}. The current I_{SC} that corresponds to the density of cesium scattering atoms in the scattering chamber was obtained by subtracting the measured background current I_{BG} at the off-center position (flag F_2 closed) from I_{SCT}. At each desired reservoir temperature (i.e., each attenuation point), a sufficient time was allowed (15 to 30 min) for a steady state to be attained. The criterion for steady state was that neither the indicated scattering chamber density nor the attenuated beam intensity at the peak should change noticeably (within a few percent) over the time required to record a datum point. At least 10 datum points were taken for each run. Each run also consisted in observing the attenuation over a full temperature cycle of the scattering chamber reservoir; that is, the attenuation line was traversed back and forth. The temperature range of the scattering chamber reservoir (0° to 70° C) provided sufficient cesium vapor density in the scattering chamber to attenuate the main cesium beam between 0 and 50 percent. Each time the cesium reservoir temperature was returned to 0° C, the total beam returned to within ±2 percent of its initial value. Typical total beam currents were of the order of 10^{-9} ampere.

Slit Alinement and Angular Resolution

The main beam profiles that were observed in the runs labeled 1, 2a, 2b, and 3 are

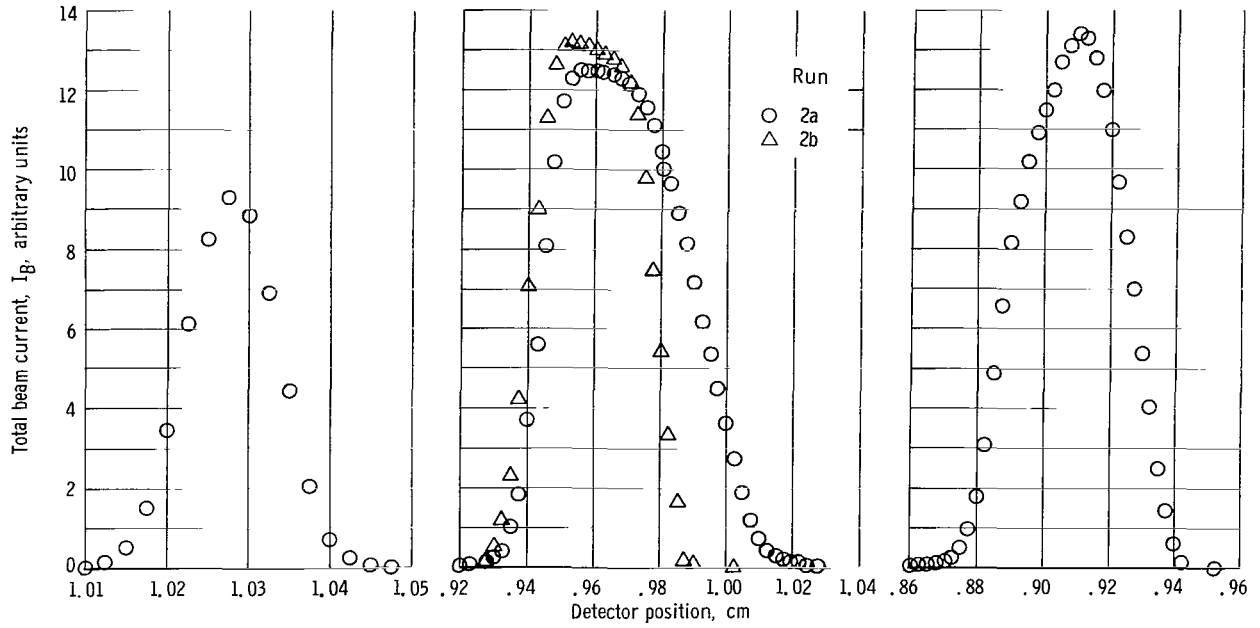

Figure 2. - Unscattered beam profile.

TABLE I. - LABORATORY ANGULAR RESOLUTION

Run	Atomic beam width at half-maximum intensity, $W_{1/2}$, cm		Angular resolution of beam apparatus, θ_L, rad
	Calculated	Experimental	
1	0.011	0.014	0.818×10^{-3}
2a	.062	.050	1.79
2b	.062	.039	1.39
3	.036	.041	2.38

presented in figure 2. A comparison of the measured and calculated widths $w_{1/2}$ at half-maximum is given in table I for these profiles. The alinement of the slits by the optical technique outlined in the preceding section was confirmed by the measured beam profiles in runs 1 and 3; however, for run 2a the observed profile was not symmetric (fig. 2(b)). This asymmetry is attributed to errors in the horizontal alinement for this run. An additional run (designated 2b and employing the same experimental setup as in run 2a, the triangular data in fig. 2(b)) was made with the collimating slit C moved into a new position such that it tended to symmetrize the beam. This was done to see if collimation near the detector plane (run 2b) had an appreciable effect on the measured partial cross section.

The experimental beam width at half-maximum $w_{1/2}$ was used to compute the angular resolution θ_L (in the laboratory system) for each run in accordance with the Kusch criterion (ref. 19). For collimation after scattering (runs 1 and 3), application of the Kusch criterion yields

$$\theta_L = \sqrt{2}\,\frac{w_{1/2}}{2}\,\frac{l_{os} + l_{sc}}{l_{sd}\left(l_{os} + \frac{l_{sc}}{2}\right)} \tag{12a}$$

For collimation before scattering (runs 2a and 2b), application of the Kusch criterion yields

$$\theta_L = \sqrt{2}\,\frac{w_{1/2}}{2}\,\frac{1}{l_{sd} + \frac{l_{sc}}{2}} \tag{12b}$$

where l_{os}, l_{sc}, and l_{sd} are defined in figure 1 (p. 9). The angular resolution θ_L for each of the runs is also given in table I.

Determination of Scattering Particle Density

As discussed earlier, the density of scattering particles participating in the collisions was determined directly at each attenuation point by an absolute measurement of the particle flux from the scattering chamber under ideal effusive flow conditions. This particle flux was converted to the actual density in the scattering chamber by means of the kinetic theory equation governing effusive flow. Kinetic theory gives the partial flow of particles Γ_a from an ideal isothermal enclosure as (Ramsey, ref. 20)

$$\Gamma_a = \frac{n\bar{v}}{4\pi} \cos\theta\, A_s\, d\Omega \tag{13}$$

In this equation Γ_a is the number of particles per second passing into the solid angle $d\Omega$ that lies at a polar angle of θ relative to the direction of the outward normal from the source area A_s, n is the density of particles per cubic centimeter distributed uniformly throughout the enclosure, and $\bar{v}$ is the mean velocity of the Maxwellian velocity distribution of the particles in thermal equilibrium with the enclosure. Equation (13) is valid if the mean free path of the effusing particles is large, as is the case considered herein, compared to the slit width and depth.

Figure 1 shows the geometry used in the present experiments. The flux Γ_a is directly measured on an absolute basis in terms of the ion current from the surface ionization detector since cesium atoms incident on a hot (~1800° K) tungsten surface are converted to ions with nearly 100-percent efficiency (Datz and Taylor, ref. 21). The

TABLE II. - PARTICLE DENSITY CONSTANT

Run	Ratio of particle density to detector current, κ	Scattering chamber temperature, T_{SC}, ^{o}K
1	13.8×10^{22}	397
2a	2.69	383
2b	2.69	383
3	4.72	383

measured particle current I_{SC} is given by

$$I_{SC} = \frac{ne\bar{v}}{4\pi} A_s \frac{A_d}{l_{sd}^2} \tag{14}$$

In this equation, I_{SC} is the measured current in amperes, and e is the charge on the electron. The solid angle $d\Omega$ has been replaced by the ratio of the detector area A_d to the square of the source to detector distance l_{sd}, and $\cos\theta$ has been set equal to 1 since the maximum lateral displacement of the detector is small compared to the distance l_{sd}. Consequently, the atom number density in the scattering chamber is given by

$$n = \kappa I_{SC} \tag{15}$$

where

$$\kappa = \frac{4\pi l_{sd}^2}{e\bar{v}A_s A_d}$$

The proportionality constant κ is dependent on the geometry of each run and also on the scattering chamber temperature through $\bar{v}$. The constant κ is presented in table II.

PARTIAL AND TOTAL CROSS SECTION

Analysis of the atomic beam attenuation data is based on the relation

$$I_B = I_0 e^{-n l_{sc} \bar{S}(0)} \tag{16}$$

where l_{sc} is the length of the scattering chamber, n is the uniform number density of target gas atoms present in the scattering chamber, I_0 is the beam current that enters the scattering chamber, I_B is the beam current that leaves the scattering chamber, and $\bar{S}(0)$ is the laboratory effective cross section for the beam-target gas pair (assuming $\theta_L = 0$). Hence, a semilogarithmic plot of I_B against n should result in a straight line

TABLE III. - ATOMIC BEAM ATTENUATION DATA

$\left[I_B = I_{BT} - I_{SCB};\ I_{SC} = I_{SCT} - I_{BG};\ n = \kappa I_{SC}\right]$

Total observed detector current with beam centered on detector sensitive area, I_{BT}, A	Current due to particle effusing from scattering chamber exit slit observed with detector sensitive area centered on beam plus detector background current, I_{SCB}, A	Total detector current in off-center position, I_{SCT}, A	Background current due to detector characteristics, I_{BG}, A
	Run 1		
0.432×10^{-10}	0.265×10^{-10}	273×10^{-13}	5.0×10^{-13}
0.575	190	202	5
1.08	.120	127	5
1.95	.060	80	5
2.43	.049	67.5	5
3.10	.035	52.5	5
3.95	.023	38.5	5
5.10	.013	23.5	5
5.74	.010	17.5	4.6
6.20	.008	12.8	4.7
6.65	.006	8.5	4.7
7.19	.005	5.6	4.7
6.50	.007	10.2	4.7
5.93	.0086	14.6	4.7
5.40	.0012	19.2	4.7
4.40	.018	30.5	4.7
3.40	.024	44.0	4.6
2.70	.040	57.5	4.6
2.08	.055	74.5	4.7
1.72	.0695	89.0	4.7
1.44	.0818	102	4.7
.685	.156	173	4.7
	Run 2a		
$12.8\cdot10^{-10}$	$0.004\cdot10^{-10}$	$4\cdot10^{-13}$	1×10^{-13}
12.1	.0106	14.2	
11.4	.025	34	
9.45	.0785	96	
8.92	.097	124	
8.01	.138	167	
7.22	.172	204	
6.12	.237	273	
4.98	.328	370	
5.20	.300	342	
5.45	.278	320	
6.70	.201	238	
10.10	.068	86	
10.70	.048	61	
13.30	.006	7	

Total observed detector current with beam centered on detector sensitive area, I_{BT}, A	Current due to particle effusing from scattering chamber exit slit observed with detector sensitive area centered on beam plus detector background current, I_{SCB}, A	Total detector current in off-center position, I_{SCT}, A	Background current due to detector characteristics, I_{BG}, A
	Run 2b		
12.6×10^{-10}	0.009×10^{-10}	11.5×10^{-13}	1×10^{-13}
12.0	.0175	22.5	
11.4	.032	42	
10.2	.060	76.5	
8.52	.112	143	
6.48	.212	253	
4.82	.337	385	
5.98	.246	290	
5.85	.252	294	
6.20	.229	271	
7.20	.172	209	
7.95	.143	177	
8.65	.112	141	
9.56	.080	103	
10.60	.049	63.5	
11.60	.027	36	
12.50	.010	13	
13.20	.003	3	
	Run 3		
13.8×10^{-10}	$0.0025\cdot10^{-10}$	$2.5\cdot10^{-13}$	2.5×10^{-13}
3.2	.305	342	2.0
4.55	.206	245	2.0
5.20	.173	208	2.0
6.40	.132	165	2.0
8.84	.065	87	2.0
9.75	.043	63	2.0
11.20	.026	36.5	2.0
12.50	.0034	3.5	2.1
5.27	.169	203	2.0
3.70	.265	301	2.1
7.14	.100	128	2.1

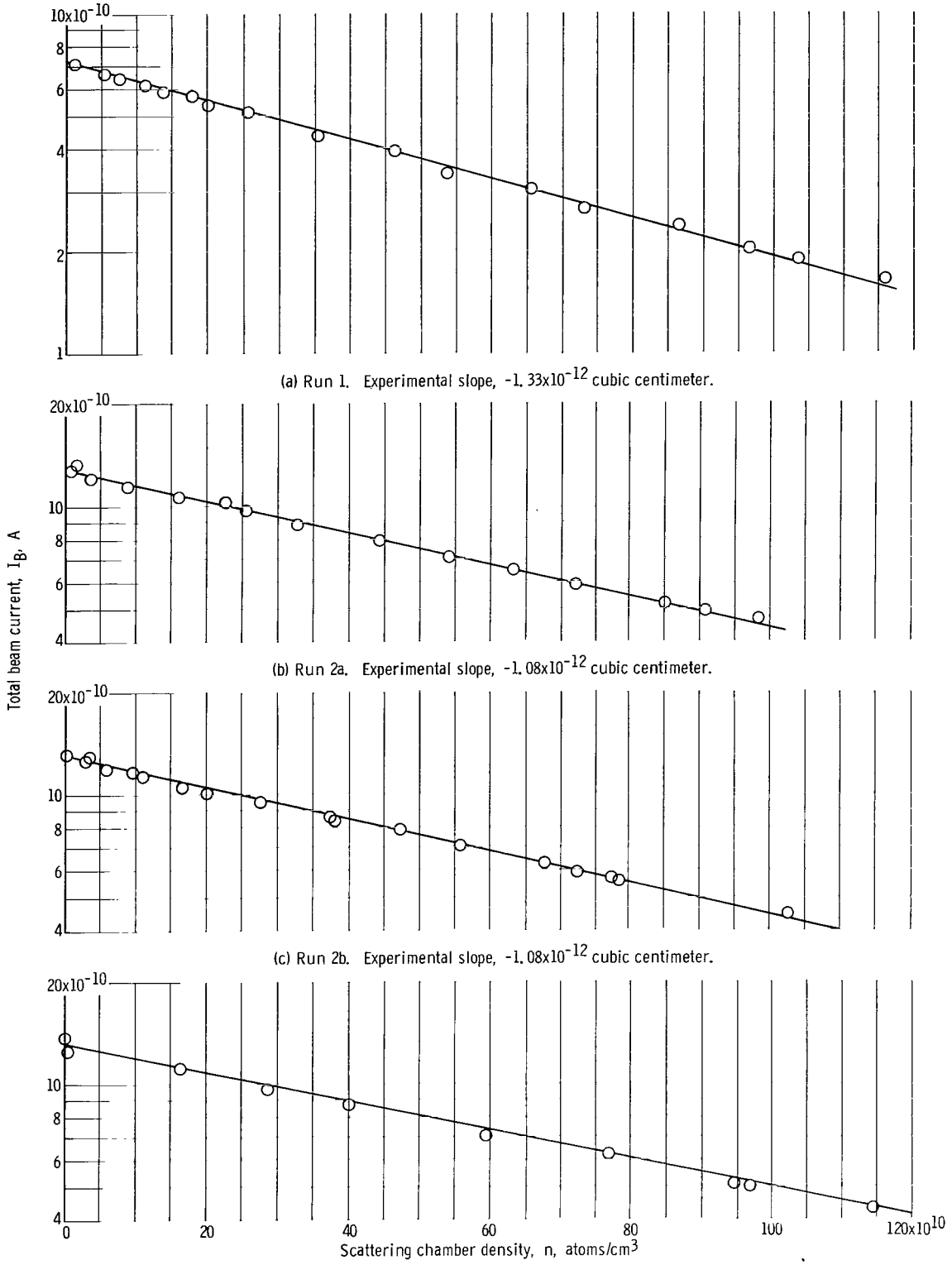

(a) Run 1. Experimental slope, $-1.33x10^{-12}$ cubic centimeter.

(b) Run 2a. Experimental slope, $-1.08x10^{-12}$ cubic centimeter.

(c) Run 2b. Experimental slope, $-1.08x10^{-12}$ cubic centimeter.

(d) Run 3. Experimental slope, $-0.96x10^{-12}$ cubic centimeter.

Figure 3. - Cesium beam attenuation.

whose slope is a measure of $\bar{S}(0)$.

The interpretation of $\bar{S}(0)$ at thermal energies requires an appropriate average of the velocity-dependent total cross section over both the beam and target gas velocity distributions (see appendix B). Berkling et al. (ref. 10) have recently established these relations for a large number of atomic beam experiments of interest. The relation they obtain between the effective cross section $\bar{S}(0)$ and the total cross section $S(0, v_{bp})$ referenced to the most probable velocity v_{bp} of the beam atoms in the oven for an experimental arrangement as used herein and for an inverse r-sixth interaction is given in the form

$$\bar{S}(0) = S(0, v_{bp})Ga_o(6, y) \tag{17}$$

where $v_{bp} = \sqrt{2kT_b/m_b}$ is the most probable velocity in the beam oven $y = v_{bp}/v_{gp}$, $v_{gp} = \sqrt{2kT_g/m_g}$ is the most probable velocity in the scattering gas, and $Ga_o(6, y)$ is the tabulated function (ref. 10) appropriate to the experiment. In the experiments reported herein, $v_{bp} = 2.3 \times 10^4$ centimeters per second, $y \cong 1.054$ and $Ga_o(6, 1.05) = 1.13$.

The analysis presented in reference 10 is strictly valid only in terms of the total cross section; that is, it gives the relation between the effective cross section $\bar{S}(0)$ in the laboratory and the actual cross section $S(0, v_{bp})$ only for those cases in which every scattering event is detected. It is assumed herein that this same analysis can be used in terms of the partial cross sections $S(\theta_L)$ (the velocity dependence in S is not indicated, since v_{bp} was a constant in this investigation). This assumption is equivalent to assuming that the velocity dependence of the partial cross section is identical to the velocity dependence of the total cross section (see appendix B).

The cesium beam attenuation data are presented in table III (p. 15) for the four runs labeled 1, 2a, 2b, and 3. These data are plotted in figures 3(a) to (d) in terms of I_B, the beam current remaining in the original beam of I_0, against n, the number density of target particles in the scattering chamber. Equation (15) was used to convert the measured scattering chamber current I_{SC} to the atom number density n. The effective partial cross section $\bar{S}(\theta_L)$ for each run was obtained from the slope M of the attenuation curve ($\bar{S}(\theta_L) = -M/l_{sc}$). The actual cross section $S(\theta_L)$ was calculated by using equation (17) (see appendix B):

$$S(\theta_L) = 0.885\, \bar{S}(\theta_L) \tag{18}$$

The partial cross sections obtained from equation (18) are plotted in figure 4 (p. 18) for the runs 1, 2a, 2b, and 3 against the square of the laboratory angular resolution θ_L. The bars are the estimated experimental error attached to each point. The point repre-

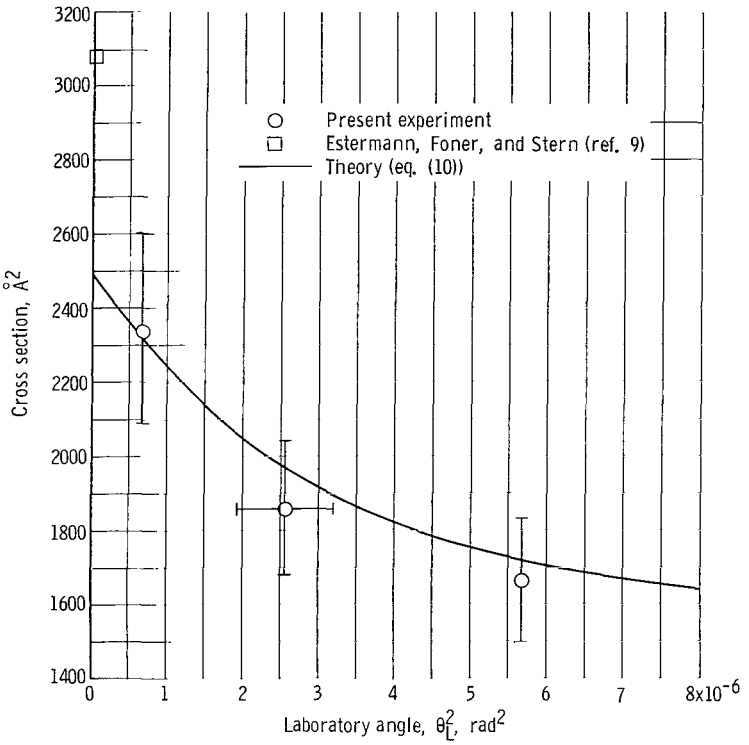

Figure 4. - Partial cross section for cesium-cesium collisions. Extrapolation to zero laboratory angular resolution.

TABLE IV. - ANGULAR RESOLUTION IN CENTER OF MASS

Run	Small angle limit for applicability of classical mechanics		Angular resolution of beam apparatus in center of mass system, θ_{cm}, rad
	θ'_c, rad (ref. 13)	θ_c, rad (ref. 15)	
1	1×10^{-3}	4×10^{-3}	1.37×10^{-3}
2a	1	4	2.65
2b	1	4	2.65
3	1	4	4.0

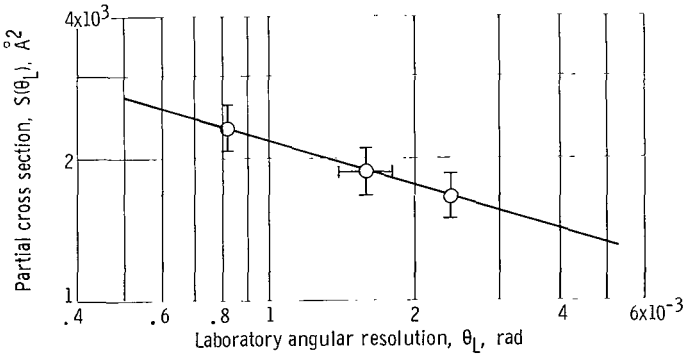

Figure 5. - Angular dependence of partial cross section. Comparison with classical theory; experimental slope -0.328; theoretical slope for s = 6, -0.333.

senting run 2 is an arithmetic mean of the runs 2a and 2b with the error bars indicating the uncertainty in the angular resolution as well as in the magnitude of the partial cross section. The data point in figure 4 attributed to Estermann et al. (ref. 9) is our reevaluation of their data on the basis of the Berkling et al. tables for an inverse r-sixth interaction.

Equation (10) is plotted in figure 4 in terms of the experimental parameters and the choice of $S(0) = 2500$ Å^2 to give a "best fit" to the experimental data. The observed dependence of these partial "total" cross sections on the angular resolution of the apparatus is seen to be in fair agreement with equation (10). Thus equation (10) provides a basis for the extrapolation of partial cross sections to zero angles to yield the true total cross section.

The angular resolutions used in these experiments are in the range between θ'_c and θ_c, the smallest angle for which classical mechanics is valid according to Mason et al. (ref. 13) and Massey and Mohr (ref. 15), respectively. These angular resolutions in the center of mass system are given in table IV. A comparison of the experimental partial cross sections presented in figure 4 with classical theory (eq. (9)) is made on a log-log plot in figure 5. Equation (9) along with the transformation to small laboratory angles (eq. (17)) predicts a linear dependence of $\log S(\theta_L)$ on $\log \theta_L$ with a slope of -0.333 for an inverse r-sixth interaction. The observed dependence is linear, which verifies the validity of classical mechanics in this angular range, and the slope of -0.328 is considered verification that the inverse r-sixth interaction is dominant at thermal energies for cesium on cesium.

The Schiff, Landau-Lifschitz approximation, $C = 5.676\times10^{-30}\, vS(0)^{5/2}$, allows the dispersion energy constant to be evaluated. When the extrapolated total cross section of 2500 Å^2 is used, a value of 4080×10^{-60} erg-cm^6 is obtained for the dispersion energy constant for the cesium-cesium interaction. This is in considerable disagreement with Fontana's theoretical value (ref. 11) of 2200×10^{-60} erg-cm^6, and it is below the value of 6900×10^{-60} erg-cm^6 calculated from the data given by Estermann et al. (ref. 9).

DIFFERENTIAL CROSS SECTION AND BEAM BROADENING

The cesium-cesium differential cross section is plotted in figure 6 (p. 20) as a function of the scattering angle in the center of mass system. The theoretical curves are calculated from equations (2) and (5) for the experimental parameters and the extrapolated values of $S(0) = 2500$ Å^2 and $K = 4080\times10^{-60}$ erg-cm^6. The limiting angles θ_c and θ'_c bracket the interval where classical and semiclassical theory overlap.

The experimental data shown in figure 6 were obtained from observed beam broaden-

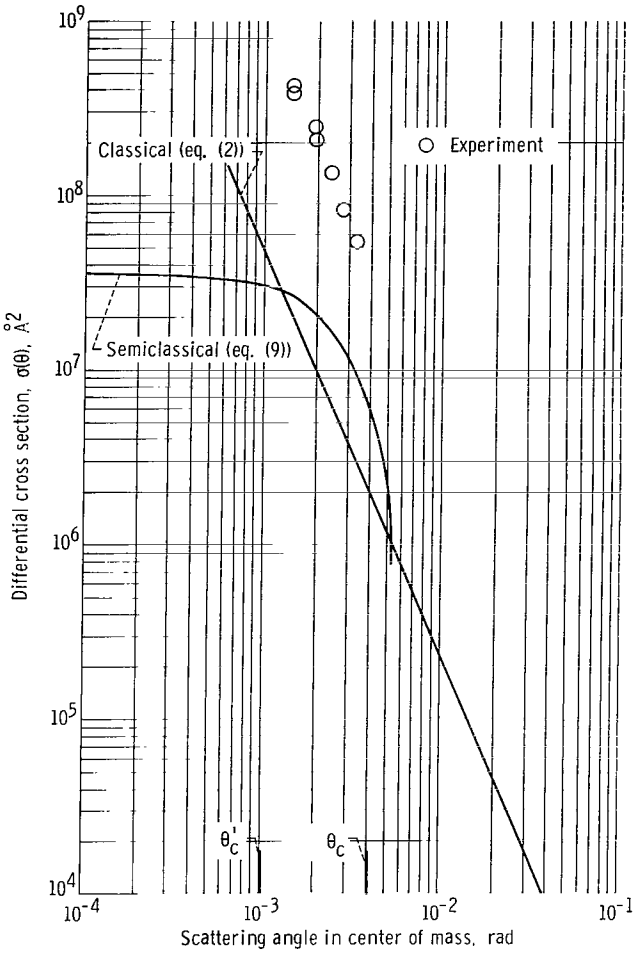

Figure 6. - Cesium-cesium differential cross section.

ing. This effect of beam broadening is shown in figure 7 where the transmitted beam profiles are presented for 28-, 61-, and 100-percent transmissions. The beam intensity at the peak has been normalized to 1 in order to display the actual broadening observed. This broadening is attributed to small angle scattering of beam atoms from their unattenuated positions in the profile over, into, and beyond the wings of the unattenuated profile.

Although the experimental setup used was not specifically designed to measure the differential cross section at small angles, a crude estimate of the absolute value of the differential cross section was made by analyzing the broadened profile corresponding to 61-percent transmission. The differential cross section $\sigma_l(\theta_l)\Delta\Omega_l$ as measured in the laboratory is given by

$$n_{sc} l_{sc} A_B \frac{I_0}{eA_d} \sigma_l(\theta_l)\Delta\Omega_l = \frac{I(\theta_l)}{e}$$

where n_{sc} is the target atom density in the scattering chamber of length l_{sc}, A_B is the beam cross sectional area in the scattering chamber, (I_0/A_d) is the equivalent beam current density in the scattering chamber, and $I(\theta_l)/e$ is the particle current detected by a detector spanning a solid angle $\Delta\Omega_l$ at a position of θ_l off the main axis of the beam. The conversion of $\sigma_l(\theta_l)$ to the differential cross section of the center of mass $\sigma(\theta)$ yields approximately

$$\sigma(\theta) \cong \frac{I(\theta_l)}{n_{sc} l_{sc} I_0 \Delta\Omega} \frac{A_d}{A_B} \tag{19}$$

where the increment of solid angle $\Delta\Omega$ in the center of mass is given for small angles θ_l by

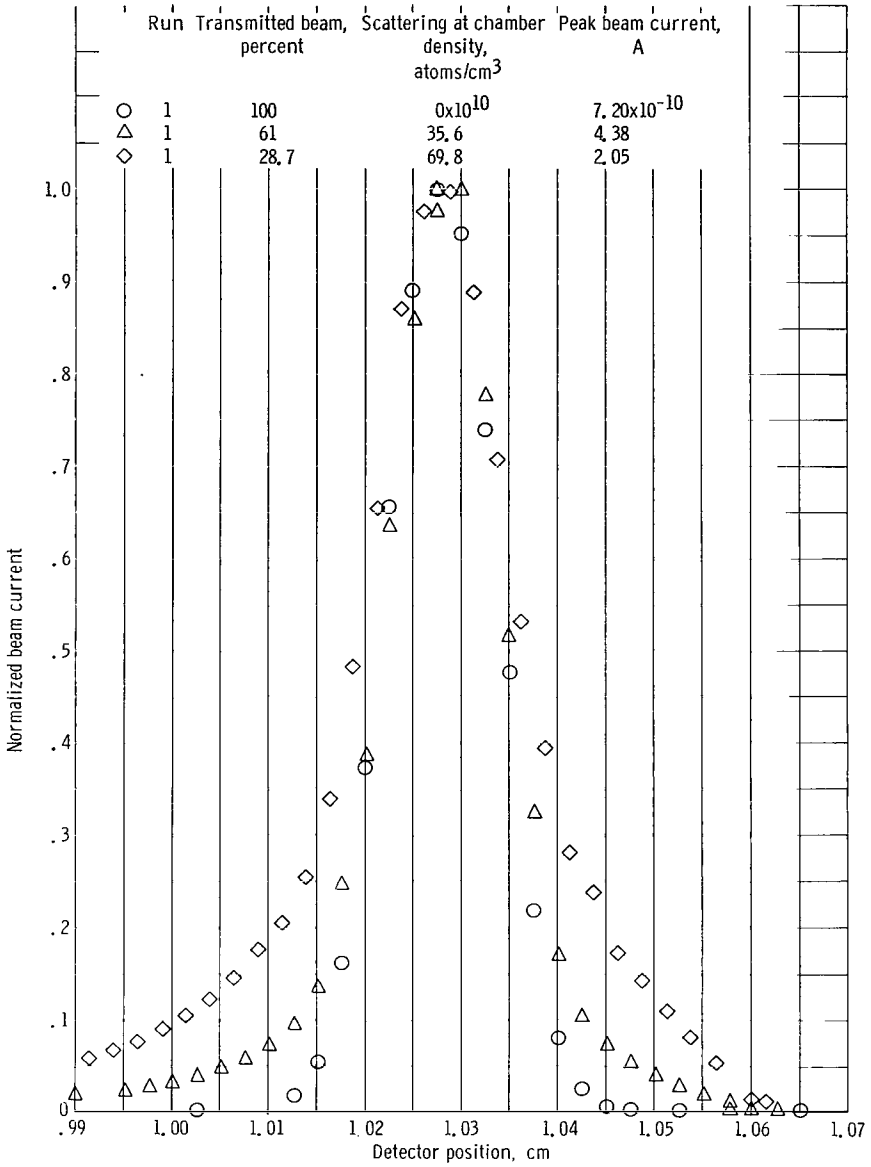

Figure 7. - Broadening of attenuated beam.

$$\Delta\Omega \cong 8\pi\theta_l \, \Delta\theta_l \left(1 + \frac{1}{2}\frac{T_g}{T_b}\right)^{-1}$$

where the approximate transformation given by equation (7) is used. Data obtained from figure 7 for 61- and 100-percent transmission were reduced according to equation (19) to the approximate values of the differential cross section shown on figure 6. It is significant that the predicted angular dependence of the differential cross section is verified by

the experiment (the data fall on a straight line).

CONCLUDING REMARKS

The value of the cesium-cesium total cross section obtained herein is 2500 $Å^2$ for an average relative velocity of 2.3×10^4 centimeters per second. Experimental evidence is presented that shows that the inverse r-sixth potential is the dominant interaction at thermal energies. A dispersion energy constant of 4080×10^{-60} erg-cm^6 is calculated from the above data†.

The cesium-cesium differential cross section at this same relative velocity is calculated in the classical-semiclassical range from the measured total cross section for an inverse r-sixth potential. The angular dependence of the calculated differential cross section is verified by semiquantitative measurements between 1×10^{-3} and 4×10^{-3} radian in the center of mass.

Both the total and differential cross section measurements verify the remark by Mason et al. (ref. 13) that classical mechanics is valid for smaller scattering angles than the lower limit given by Massey and Mohr (ref. 15).

National Aeronautics and Space Administration,
Lewis Research Center,
Cleveland, Ohio, September 2, 1965.

---

†Since this note was written Buck and Pauly (ref. 22) have reported the total cross section and dispersion energy constant for cesium-cesium collisions as well as other alkali-alkali combinations. They obtain a value of 2300 $Å^2$ for a reference velocity of 2.3×10^4 cm/sec. This is in fair agreement with the value obtained herein of 2500 $Å^2$, but disagrees as does this work with the Estermann et al. value of 3090 $Å^2$.

APPENDIX A

SYMBOLS

A	spin statistical parameter
A_B	beam cross-sectional area
A_d	detector sensitive area
A_s	source area
C	dispersion energy constant (equals K for potential with $s = 6$)
C_s	gamma function ratio, $\pi\Gamma\left(\frac{s+1}{2}\right)\Big/\Gamma\left(\frac{s}{2}\right)$
e	electron charge
$f(\theta)$	scattering amplitude
$f(6)$	constant, $\frac{\left[\Gamma\left(\frac{2}{5}\right)\right]^2}{\Gamma\left(\frac{4}{5}\right)}\tan\left(\frac{2\pi}{5}\right)$
$Ga_o(6,y)$	Berking et al. (ref. 10) tabulated function
$\hbar$	Planck's constant divided by 2π
I_B	beam current
I_{BG}	background current due to detector characteristics
I_{BT}	total observed detector current with beam centered on detector sensitive area
I_{SC}	portion of I_{SCT} due to particles effusing from scattering chamber exit slit when detector is in off-center position
I_{SCB}	current due to particle effusing from scattering chamber exit slit observed with detector sensitive area centered on beam plus detector background current
I_{SCT}	total detector current in off-center position
$I(\theta_l)$	beam current scattered into element of solid angle $\Delta\Omega_l$ at θ_l off beam axis
I_0	beam particle current entering scattering chamber
K	interaction potential constant
k	Boltzmann's constant, when followed by T
k	wave number, $\mu v/\hbar$
l_{os}	distance from oven slit to scattering chamber entrance
l_{sc}	length of scattering chamber
l_{sd}	distance from scattering chamber exit slit to detector
M	slope of experimental attenuation curve

m_b	beam atomic mass
m_g	scattering gas atomic mass
n	particle density
n_{sc}	scattering gas atom number density
Q	experimental cross section, cm^2
r	interatomic distance
S(0)	total cross section
$\bar{S}(0)$	laboratory effective cross section
$S_{(0, v_{bp})}$	total cross section at most probable velocity of beam atoms in oven
$S(\theta)$	partial cross section
s	exponent on r in interaction potential
T	temperature
T_b	beam atom temperature
T_g	scattering gas temperature
T_{SC}	scattering chamber temperature
V(r)	interaction potential
v	relative velocity of collision
$\bar{v}$	Maxwellian average velocity
v_{bp}	most probable speed of a beam atom in oven
v_{gp}	most probable speed of a scattering gas atom
$\langle v_r \rangle$	relative velocity averaged over colliding particle velocity distributions
$w_{1/2}$	atomic beam width at half-maximum intensity
x	beam atom reduced velocity, $v_b / \sqrt{m_b/2kT_b}$
y	velocity ratio, v_{bp}/v_{gp}
z	gas atom reduced velocity, $v_g / \sqrt{m_g/2kT_g}$
α	temperature ratio, T_g/T_b
Γ	gamma function
Γ_a	particle flow rate into element of solid angle $d\Omega$ at polar angle θ
ϵ	relative energy of collision, $\mu \langle v_r \rangle^2/2$
θ	scattering angle in center of mass system; polar angle
θ_c	small angle limit for applicability of classical mechanics according to Massey and Mohr (ref. 15)
θ'_c	small angle limit for applicability of classical mechanics according to Mason, Vanderslice, and Raw (ref. 13)
θ_{cm}	angular resolution of the beam apparatus in the center of mass system

θ_L	angular resolution of beam apparatus
$\langle\theta_L^2\rangle$	square of angular resolution in laboratory system corresponding to θ_{cm}^2 in center of mass system averaged over velocity distributions of colliding particles
θ_l	scattering angle in laboratory system
κ	ratio of particle density to detector current
μ	reduced mass of colliding atoms, $m_b m_g/(m_b + m_g)$
$\sigma(\theta)$	differential cross section in center of mass system
$\sigma_l(\theta_l)$	differential cross section in laboratory system
ψ	angle between velocity vectors $\vec{v}_b$ and $\vec{v}_g$
Ω	solid angle in center of mass system
Ω_l	solid angle in laboratory system

APPENDIX B

EFFECTIVE AND PARTIAL CROSS SECTION

The effective total cross section $\bar{S}(0)$ introduced in equation (16) is given by Berkling et al. (ref. 10) in the form

$$\bar{S}(0, v_{bp}, v_{gp}) = \int_{\vec{v}_g} \int_{\vec{v}_b} F_g(\vec{v}_g, v_{gp}) F_b(\vec{v}_b, v_{bp}) \frac{v(\vec{v}_g, \vec{v}_b)}{v_b} S(0, v) \cdot d\vec{v}_b \, d\vec{v}_g \qquad \text{(B1)}$$

where $v = |\vec{v}_b - \vec{v}_g|$. Equation (B1) is for a perfectly collimated beam with velocity distribution $F_b(\vec{v}_b, v_{bp})$ being scattered by an isotropic scattering gas with velocity distribution $F_g(\vec{v}_g, v_{gb})$. It is assumed in the derivation of equation (B1) that every scattering event is detected (apparatus has zero angular resolution).

Then it is shown (ref. 10) that equation (B1) may be given by

$$\bar{S}(0, v_{bp}, v_{gp}) = Ga_o\left(s, \frac{v_{bp}}{v_{gp}}\right) S(0, v_{bp})$$

where the velocity dependence of $S(0, v)$ is assumed to be of the form

$$\text{constant}\left(\frac{1}{v}\right)^{\frac{2}{s-1}}$$

with s representing the exponent on r in the interaction potential. Berkling et al. (ref. 10) tabulated the function

$$Ga_o\left(6, \frac{v_{bp}}{v_{gp}}\right)$$

An atomic beam apparatus does not have zero angular resolution as assumed in the Berkling et al. calculations; it will have some finite polar angular resolution θ_L. Then equation (B1) must be written

$$S(\theta_L, v_{bp}, v_{gp}) = \int_{\vec{v}_b} \int_{\vec{v}_g} \int_{\theta_L}^{\pi} F_b(\vec{v}_b, v_{bp}) F_g(\vec{v}_g, v_{gp}) \frac{v(\vec{v}_b, \vec{v}_g)}{v_b} 2\pi\sigma_e(\theta_e, v) \sin\theta_e \, d\theta_e \, d\vec{v}_b \cdot d\vec{v}_g \tag{B2}$$

From the definition of partial cross section,

$$S(\theta_L, v) = \int_{\theta_L}^{\pi} 2\pi\sigma_e(\theta_e, v) \sin\theta_e \, d\theta_e \tag{B3}$$

If the partial cross section is assumed to have the same velocity dependence as the total cross section, then

$$\bar{S}(\theta_L, v_{bp}, v_{gp}) \simeq Ga_o\left(6, \frac{v_{bp}}{v_{gp}}\right) S(\theta_L, v_{bp}) \tag{B4}$$

This expression is used to obtain equation (18) of the text.

One can also write the partial cross section as

$$S(\theta_{cm}, v) = \int_{\theta_{cm}}^{\pi} 2\pi\sigma(\theta, v) \sin\theta \, d\theta \tag{B5}$$

where

$$S(\theta_L, v) \simeq S(\theta_{cm}, v) \tag{B6}$$

when θ_L and θ_{cm} are related by equation (7).

The measured effective cross section and equation (B4) are used to determine $S(\theta_L, v)$. The theoretical calculations yield $S(\theta_{cm}, v)$, and comparisons of theory and experiment are made on the basis of equation (B6).

APPENDIX C

COORDINATE TRANSFORMATION

The relation between a small scattering angle θ_L in the laboratory system and the average scattering angle θ_{cm} in the center of mass system (eq. (7)) is derived herein for the following special case:

(1) Central forces (conservation of angular momentum)

(2) Elastic collisions

(3) Equal mass collision partners

(4) Maxwellian-type velocity distributions in the beam and the scattering gas

The kinematic problem is shown in sketch (e) where subscripts b and g refer to beam and scattering gas particles, respectively. The beam velocity $\vec{v}_b$ is held fixed in direction in the laboratory. However, its magnitude can vary in accordance with the velocity distribution present in the beam. The scattering gas velocity $\vec{v}_g$ intersects $\vec{v}_b$ at an angle ψ. The magnitude of $\vec{v}_g$ can vary in accordance with the velocity distribution present in the scattering gas and ψ can vary from 0 to π. The gas atom velocity can also vary over 2π in azimuthal angle; however, this has no effect on the polar angle θ_L for this special case. The relative velocity $\vec{v}_r$ is given by $\vec{v}_r = \vec{v}_b - \vec{v}_g$. The magnitude of $\vec{v}_r$ is unchanged in the collision, but it's direction is shown rotated by θ_{cm} (counterclockwise rotations are positive) in the center of mass. Application of the laws of energy and momentum conservation yields after some algebraic manipulation

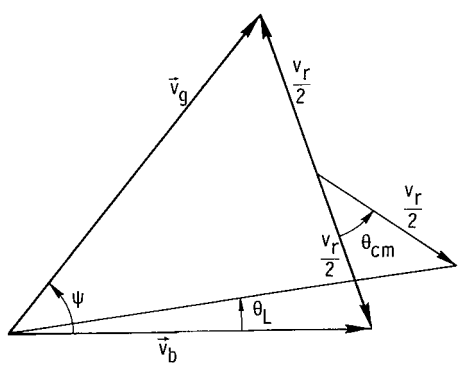

(e)

$$\cos\theta_L = \frac{x(1+\cos\theta_{cm}) + z\alpha\left[\cos\psi(1-\cos\theta_{cm}) + \sin\psi\sin\theta_{cm}\right]}{\left[2(x^2+z^2\alpha^2) + 2(x^2-z^2\alpha^2)\cos\theta_{cm} + 4\alpha xz\sin\psi\sin\theta_{cm}\right]^{1/2}} \qquad \text{(C1)}$$

where x and z are the reduced velocities

$$x = v_b\sqrt{\frac{m_b}{2kT_b}}$$

and

$$z = v_g \sqrt{\frac{m_g}{2kT_g}}$$

of the beam and scattering gas, respectively, and

$$\alpha^2 = \frac{T_g}{T_b}$$

Assuming $\theta_{cm} \ll 1$, $\theta_L \ll 1$ and keeping terms to order θ_{cm}^2 and θ_L^2, one obtains from equation (C1) the following approximate expression:

$$\theta_L^2 \simeq \frac{\theta_{cm}^2}{4} - \frac{\alpha z}{x}\frac{\theta_{cm}^2}{2}\cos\psi + \frac{\alpha^2 z^2}{x^2}\frac{\theta_{cm}^2}{4}\cos^2\psi \qquad \text{(C2)}$$

The averaging of each side of equation (C2) over the velocity distributions of the colliding particles is accomplished by operating with

$$\frac{4}{\sqrt{\pi}} \int_{x=0}^{\infty} \int_{z=0}^{\infty} \int_{\psi=0}^{\pi} x^3 e^{-x^2}\, dx\, z^2 e^{-z^2}\, dz \sin\psi\, d\psi$$

The result of the above integrations yields

$$\langle \theta_L^2 \rangle = \frac{\theta_{cm}^2}{4}\left(1 + \frac{1}{2}\frac{T_g}{T_b}\right) \qquad \text{(C3)}$$

which is equation (7) of the text.

REFERENCES

1. Bernstein, R.B.: Molecular Beam Scattering at Thermal Energies. Science, vol. 144, no. 3615, Apr. 10, 1964, pp. 141-150.

2. Pauly, H.: Scattering Experiments on Molecular Beams and Intermolecular Forces. Fortschr. Physik, vol. 9, 1961, pp. 613-687.

3. Rothe, Erhard W.; and Bernstein, Richard B.: Total Collision Cross Sections for the Interaction of Atomic Beams of Alkali Metals with Gases. J. Chem. Phys., vol. 31, no. 6, Dec. 1959, pp. 1619-1627.

4. Rothe, Erhard W.; Marino, Lawrence L.; Neynaber, R.H.; Rol, P.K.; and Trujillo, S.M.: Scattering of Thermal Rare Gas Beams by Argon. Influence of the Long-Range Dispersion Forces. Phys. Rev., vol. 126, no. 2, Apr. 15, 1962, pp. 598-602.

5. Pauly, H.: Further Cross-Sections for Collisions Between Atoms. Angew. Phys., vol. 9, no. 12, Dec. 1957, pp. 600-606.

6. Ishii, H.; and Nakayama, K.: A Serious Error Caused by Mercury Vapor Stream in the Measurement with a McLeod Gauge in the Cold Trap System. (Effect of the Diffusion of Nitrogen in the Mercury Vapor Stream.) Trans. Eighth Nat. Vacuum Symposium, Vol. 1, Pergamon Press, 1962, pp. 519-524.

7. Meinke, C.; and Reich, G.: Influence of Diffusion on the Measurement of Low Pressure with the McLeod Vacuum Gauge. Vacuum, vol. 13, 1963, pp. 579-581.

8. Pauly, Hans: Die Kleinwinkelstreuung bei Stössen zwischen neutralen Atomen. Z. Physik, bd. 157, 1959, pp. 54-64.

9. Estermann, I.; Foner, S.N.; and Stern, O.: The Mean Free Paths of Cesium Atoms in Helium, Nitrogen, and Cesium Vapor. Phys. Rev., vol. 71, no. 4, Feb. 15, 1947, pp. 250-257.

10. Berkling, K.; Helbing, R.; Kramer, K.; Pauly, H.; Schlier, Ch.; und Toschek, P.: Effektive Stossquerschnitte bei Streuversuchen. Z. Physik, bd. 166, 1962, pp. 406-428.

11. Fontana, Peter R.: Theory of Long-Range Interatomic Forces. 1. Dispersion of Energies Between Unexcited Atoms. Phys. Rev., vol. 123, no. 5, Sept. 1, 1961, pp. 1865-1870.

12. Bernstein, R.B.: Elastic Scattering of Atoms and Molecules in the Thermal Energy Range. Proc. Third Int. Conf. Phys. of Electronic and Atomic Collisions, John Wiley & Sons, Inc., 1964, pp. 895-913.

13. Mason, E.A.; Vanderslice, J.T.; and Raw, C.F.G.: Quantum Effects in Small-Angle Molecular-Beam Scattering. J. Chem. Phys., vol. 40, no. 8, Apr. 15, 1964, pp. 2153-2164.

14. Davies, R.H.; Mason, E.A.; and Munn, R.J.: High-Temperature Transport properties of Alkali Metal Vapors. Phys. Fluids, vol. 8, no. 3, Mar. 1965, pp. 444-452.

15. Massey, H.S.W.; and Mohr, C.B.O.: Free Paths and Transport Phenomena in Gases and the Quantum Theory of Collisions. II. The Determination of the Laws of Force Between Atoms and Molecules. Proc. Roy. Soc. (London), ser. A, vol. 144, no. 851, Mar. 1, 1934, pp. 188-204.

16. Ford, K.W.; and Wheeler, J.A.: Semiclassical Description of Scattering. Annals of Phys., vol. 7, 1959, p. 259.

17. Manista, E.J.; and Sheldon, J.W.: Preliminary Experiments with a Velocity-Selected Atomic-Beam Apparatus. NASA TN D-2557, 1964.

18. Manista, E.J.; and Sheldon, J.W.: Influence of Opposing Slits on Molecular Flow from an Isothermal Enclosure at Low Densities. NASA TN D-2986, 1965.

19. Kusch, P.: Notes on Resolution in Scattering Measurements. J. Chem. Phys., vol. 40, no. 1, Jan. 1, 1964, pp. 1-4.

20. Ramsey, N.F.: Molecular Beams. Clarendon Press (Oxford) 1956.

21. Datz, Sheldon.; and Taylor Ellison H.: Ionization on Platinum and Tungsten Surfaces. I. The Alkali Metals. J. Chem. Phys., vol. 25, no. 3, Sept. 1956, pp. 389-394.

22. Buck, U.; und Pauly, H.: Messungen des van der Waals-Potentials Zwischen Alkaliatomen. Z. Physik, bd. 185, 1965, pp. 155-168.

"The aeronautical and space activities of the United States shall be conducted so as to contribute . . . to the expansion of human knowledge of phenomena in the atmosphere and space. The Administration shall provide for the widest practicable and appropriate dissemination of information concerning its activities and the results thereof."

—NATIONAL AERONAUTICS AND SPACE ACT OF 1958

NASA SCIENTIFIC AND TECHNICAL PUBLICATIONS

TECHNICAL REPORTS: Scientific and technical information considered important, complete, and a lasting contribution to existing knowledge.

TECHNICAL NOTES: Information less broad in scope but nevertheless of importance as a contribution to existing knowledge.

TECHNICAL MEMORANDUMS: Information receiving limited distribution because of preliminary data, security classification, or other reasons.

CONTRACTOR REPORTS: Technical information generated in connection with a NASA contract or grant and released under NASA auspices.

TECHNICAL TRANSLATIONS: Information published in a foreign language considered to merit NASA distribution in English.

TECHNICAL REPRINTS: Information derived from NASA activities and initially published in the form of journal articles.

SPECIAL PUBLICATIONS: Information derived from or of value to NASA activities but not necessarily reporting the results of individual NASA-programmed scientific efforts. Publications include conference proceedings, monographs, data compilations, handbooks, sourcebooks, and special bibliographies.

Details on the availability of these publications may be obtained from:

SCIENTIFIC AND TECHNICAL INFORMATION DIVISION

NATIONAL AERONAUTICS AND SPACE ADMINISTRATION

Washington, D.C. 20546